Cell. Mol. Life Sci. (2015) 72:885–896
DOI 10.1007/s00018-014-1825-7

Cellular and Molecular Life Sciences

MULTI-AUTHOR REVIEW

Spectroscopic and computational characterization of laccases and their substrate radical intermediates

Rebecca Pogni · Maria Camilla Baratto · Adalgisa Sinicropi · Riccardo Basosi

Received: 23 December 2014 / Accepted: 30 December 2014 / Published online: 17 January 2015

Abstract Laccases are multicopper oxidases which oxidize a wide variety of aromatic compounds with the concomitant reduction of oxygen to water as by-product. Due to their high stability and biochemical versatility, laccases are key enzymes to be used as eco-friendly biocatalyst in biotechnological applications. The presence of copper paramagnetic species in the catalytic site paired with the substrate radical species produced in the catalytic cycle makes laccases particularly attractive to be studied by spectroscopic approaches. In this review, the potentiality of a combined multifrequency electron paramagnetic spectroscopy /computational approach to gain information on the nature of the catalytic site and radical species is presented. The knowledge at molecular level of the enzyme oxidative process can be of great help to model new enzymes with increased efficiency and robustness.

Keywords Multicopper oxidases · Copper catalytic site · Laccase's catalytic mechanism · Substrate oxidation · Paramagnetic species · Radical intermediates · EPR spectroscopy · DFT calculations

Introduction

Laccases, as a family of copper-containing oxidases, are widely distributed in nature and utilize the unique redox property of the copper ion to oxidize a wide variety of substrates. Since their discovery in 19th century, these enzymes have been the subject of increasing research and represent the most important biocatalysts for biotechnological applications [1, 2]. Laccases are able to oxidize directly polyphenols, polyamines, ortho- and para-diphenols as well as aryl diamines [3–5].The oxidative cycle involves the production of four substrate radical species paired with the use of molecular oxygen as electron acceptor. The water is the only by-product of the reaction [6].

Laccases have different redox potentials depending on their sources. Indeed, plant and bacterial laccases exhibit the lower value ($\sim$0.4 V) while the fungal laccases exhibit the higher one ($\sim$0.8 V) [7].

The mechanism for substrate oxidation is based on the Marcus "outer sphere" theory where the difference in redox potential, ΔE_0, determining the electron transfer rate, is the driving force [8–10].

The technological potential of laccases has long been recognized and numerous studies of their use in various bioconversion processes have been performed [11]. Above all, fungal laccases, for their role in lignin biodegradation, show very strong oxidative properties [12, 13]. Nonetheless, their action would be restricted to the oxidation of small phenolic compounds (like the phenolic lignin moieties), as non-phenolic substrates, with a redox potential above 1.3 V or big substrate molecules (which have no access to the active site for steric constraints), cannot be oxidized directly by laccase. The research on laccases was pushed forward with the description of certain synthetic compounds able to oxidize more recalcitrant non-phenolic substrates by laccase-mediator system [14]. Indeed, mimicking nature, these small organic molecules, once oxidized, can diffuse in solution as electron shuttles to oxidize in turn complex substrate molecules. As a result of the laccase oxidation process, radicals can be generated either on substrates or mediator molecules and then these

R. Pogni · M. C. Baratto · A. Sinicropi · R. Basosi (✉)
Department of Biotechnology, Chemistry and Pharmacy, University of Siena, Via A Moro 2, 53100 Siena, Italy
e-mail: riccardo.basosi@unisi.it

species can undergo the formation of a quinonoid derivative or intermolecular nucleophilic attack by itself to produce homomolecular dimers [11, 15–17]. In some cases, depending on the nature of the precursors or radical chemistry, oligomers, polymers, and new heteromolecular hybrid molecules can be generated [11, 18]. Laccases have been reviewed many times and spectroscopic and computational techniques have provided significant insights into the molecular mechanisms of these copper enzymes [19–28].

Considering the great amount of the paramagnetic species present in the catalytic cycle of laccases, this review focuses mainly on their identification and characterization with emphasis on the relevant role of a combined use of the electron paramagnetic resonance spectroscopy (EPR) and computational methods. These studies allow one to obtain straightforward information on the catalytic mechanism of these enzymes. The modeling of new enzymes with improved characteristics will significantly benefit from the acquired knowledge on the catalytic mechanism.

EPR characterization of T1 and T2 copper sites in Laccases

EPR spectroscopy is a useful tool for the study and structural characterization of the Cu(II) metal centers present in the prosthetic group of the enzyme. The unpaired electron located in the $d_{x^2-y^2}$ orbital produces a characteristic $S = ½$ EPR spectrum with $g_{\|} > g_{\perp} > 2.0023$. The two naturally copper isotopes ^{63}Cu and ^{65}Cu (69 and 31 % respectively) have a nuclear spin $I = 3/2$ which couples with the unpaired electron giving a $2I + 1$ or four-line hyperfine splitting of the EPR signal [29]. The T1 site is characterized by an intense absorption at $\sim$600 nm and $\varepsilon \sim 5{,}000\ M^{-1}\ cm^{-1}$ due the ligand to metal charge transfer, S(Cys)$\pi \rightarrow$ Cu $d_{x^2-y^2}$ transition, responsible for the intense blue color of the oxidized form of the enzyme [21–23]. They also exhibit a very small Cu parallel hyperfine splitting [$A_{\|} = (43–90) \times 10^{-4}\ cm^{-1}$] in the EPR spectra. The trinuclear center, where dioxygen is reduced to water, is comprised of one T2 copper ion and a coupled binuclear copper center, T3. The two copper ions in the T3 site, which are usually antiferromagnetically coupled through a bridging ligand and therefore EPR silent, show a characteristic absorption band at 330 nm. The T2 site lacks strong absorption bands, and exhibit a large parallel hyperfine splitting in the EPR spectra [$A_{\|} = (150–201) \times 10^{-4}\ cm^{-1}$]. Laccase has an EPR spectrum indicating the presence of a combination of T1 and T2 copper centers while the T3 center is EPR inactive.

A multifrequency EPR approach is important for a complete and clear characterization of the copper species through the assignment of the magnetic parameters g and A [30, 31]. The EPR spectrum of the enzyme in the native state is characterized by a parallel and a perpendicular region [13, 32], as reported in Fig. 1 that represents the EPR spectra of *Coriolopsis gallica* laccase recorded at three different frequency values (S-, X-, W-band) [33]. In the parallel region of the X-band EPR spectrum (Fig. 1b), the signals of the detectable copper ions are superimposed: the four parallel components of the T1 site are evident and resolved and one parallel component of the T2 center is visible. The T1 and T2 signals of the perpendicular region are completely overlapped. At high frequency (W-band) (Fig. 1c), there is a change in the lineshape and the T1 and T2 contributions are well separated in terms of $g_{\|}$ and $g_{\perp}$, even though the hyperfine structure of T1 is not resolved because of A strain responsible of line broadening [34, 35]. At lower frequency (S-band), the hyperfine coupling constants are more easily detectable and the first and last parallel components of T2 copper center are visible (Fig. 1a) [36]. Therefore, the advantage in the use of the multifrequency EPR is to determine the g anisotropy at W-band, where the $g_{\|}$ and $g_{\perp}$ values can be directly measured on the experimental spectrum, while lower frequencies (S-band) are more suited to get the hyperfine coupling constant A. This approach leads to a unique set of magnetic parameters for an exact characterization of the paramagnetic species. The magnetic parameters that (contemporary) simulate all spectra at the three different frequencies are $g_{\|} = 2.193$, $g_{\perp} = 2.044$, $A_{\|} = 10.24$ mT, and $A_{\perp} = 0.93$ mT for T1 and $g_{\|} = 2.258$, $g_{\perp} = 2.043$, $A_{\|} = 21.40$ mT, and $A_{\perp} = 0.22$ mT for T2. The error on g values is $\pm$ 0.0001 and on A is $\pm$0.003 mT [33].

An exception to the typical lineshape of laccase EPR spectrum was obtained with the hyperthermophilic archaeon *Pyrobaculum aerophilum* (McoP) [38]. From a spectroscopic analysis, the as-isolated enzyme was found to be partially copper depleted, containing 3.2 mol of copper per mol of protein instead of the expected 4:1 ratio. The continuous wave (CW) X-band EPR spectrum of the McoP shows that the as-isolate form is in a T2-depleted form, and exogenous copper is required to achieve full activity. The CW X-band spectrum paired with its best simulation is reported in Fig. 2 and it shows a lineshape typical of a T1 copper contribution (Fig. 2a) with the magnetic parameters $g_{\|} = 2.224 \pm 0.001$ and $A_{\|} = (6.9 \pm 0.1)$ mT; no evidence of the T2 site copper is present. After the addition of exogenous copper, the T2 contribution appeared (Fig. 2b) and the spin Hamiltonian magnetic parameters $g_{\|} = 2.258 \pm 0.001$ and $A_{\|} = (17.4 \pm 0.1)$ mT were obtained simulating the experimental spectrum of McoP incubated with exogenous Cu(II) subtracted from the as-isolated McoP where only the T1 contribution was found [38].

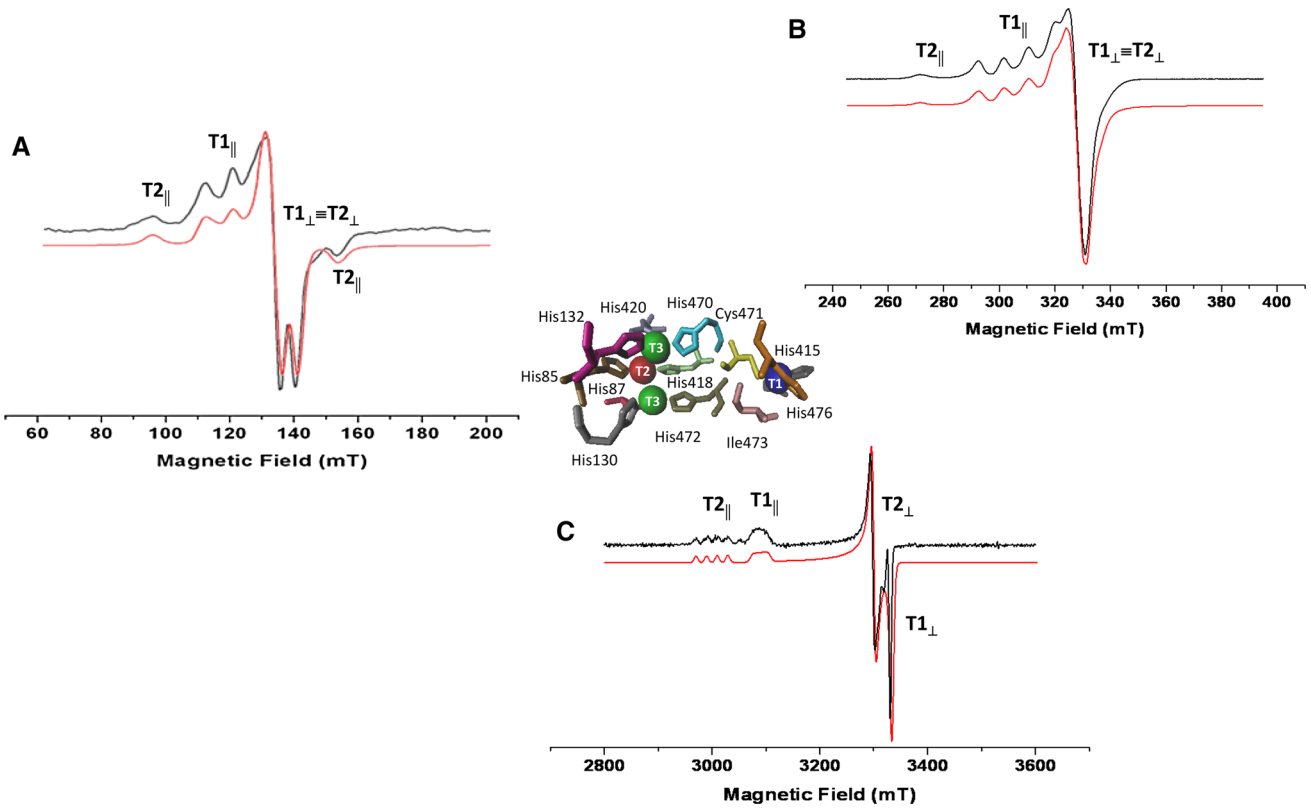

Fig. 1 CW-EPR spectra of *Coriolopsis gallica* laccase (*black line*) paired to the best simulation (*red line*) at: **a** S-band (3.83 GHz), **b** X-band (9.40 GHz), **c** W-band (94.8 GHz). Experimental conditions: 0.5 mT modulation amplitude, 20 mW microwave power, 70 K. In the center, catalytic Cu(II) sites of *Coriolopsis gallica* laccase from the crystallographic structure (pdb code: 4A2F [37]). Adapted from Martorana et al. [33]

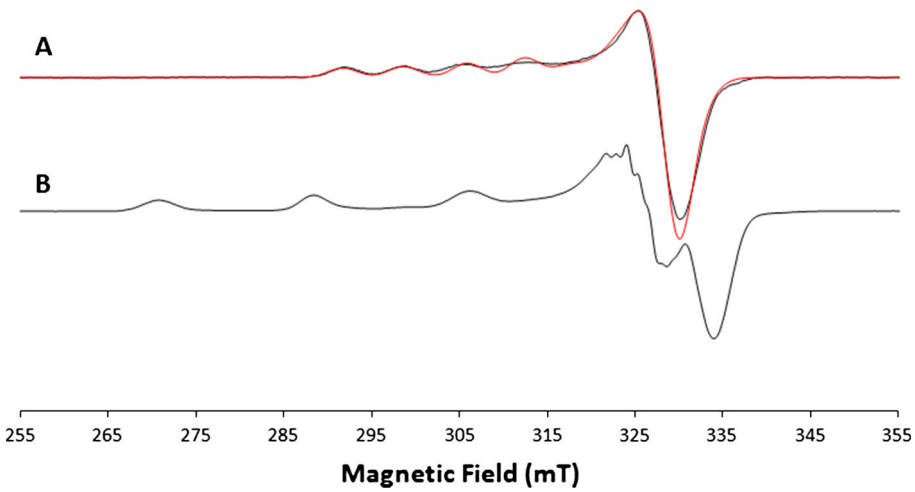

Fig. 2 CW X-band EPR spectrum of: **a** as-isolated McoP (*black line*) paired to its best simulation (*red line*); **b** McoP incubated with five equivalents of Cu(II). Experimental conditions: $\nu = 9.4$ GHz, 2 mW microwave power, 0.5 mT modulation amplitude. Adapted from Fernandes et al. [38]

Combined EPR and PCM/DFT characterization of Laccase's substrates radical intermediates

In several cases, laccases are not able to directly oxidize the substrate, due to the substrate high redox potential (>1.5 V) or to inaccessibility to the enzyme active site similarly to what occurs in nature with lignin. To oxidize the phenolic lignin unit, the enzyme uses natural mediators as electronic shuttles between the laccase and the substrate. The oxidized mediator, usually a small organic molecule, diffuses away from the enzymatic catalytic site and it oxidizes either very bulky substrates or molecules with redox potential >0.88 V [39]. Several compounds have been synthesized and used as laccase mediators despite the

fact that they are expensive, the by-product toxicity and the large mediator/substrate molar ratio strongly limit their applicability. 2,2′-azino-bis-(3-ethylbenzothiazoline-6-sulfonic acid (ABTS), violuric acid (VIO), 4-methylamino benzoic acid, 2,2′,6,6′-tetramethylpiperidine-N-oxyl (TEMPO), and 1-hydroxybenzotriazole (HBT) are only few examples of such molecules [40–46].

It is known that oxidation of mediators takes place following two different mechanisms: an electron transfer pathway (ET route) or an H-abstraction pathway (HAT route) forming, in both cases, a radical species as final product. Structural characterization of the radical intermediates and mechanistic studies of the possible pathways are of great help in understanding the mechanism for the interaction of a laccase, mediator and substrate at a molecular level, playing an important role in the improvement of these enzymes for biotechnological applications. To date, however, the radical species of only few redox mediators/precursors (ABTS, VIO, 4-methylamino benzoic acid) have been characterized by means of multifrequency EPR spectroscopy and related pulse techniques such as electron nuclear double resonance spectroscopy (ENDOR), combined with density functional theory (DFT) calculations [47, 48]. In the following, the main results of such studies are presented.

ABTS

The ABTS mediator represents the prototype of the synthetic mediator class. It is the compound most used to test the oxidative activity in many enzymes. ABTS was first investigated by CW-EPR in liquid solution using chemical processes for radical formation [49–51]. More recently, the cationic ABTS radical, formed by a fungal laccase, has been completely characterized by a combined use of multifrequency EPR, pulse ENDOR, and DFT techniques [47]. Figure 3 shows the room temperature EPR spectrum of the $ABTS^{+\bullet}$ paired with its better simulation (left) and the DFT computed spin density distribution (right). The magnetic parameters of the quite complex pattern of the EPR spectrum have been assigned by the spectral simulation assisted by the DFT calculations. The bulk solvent effects have been taken into account using the polarisable continuum model (PCM) by embedding the molecules under investigation using a dielectric constant value of $\varepsilon = 78.39$, corresponding to water. The B3LYP g-tensor values, hfcc, and Mulliken spin densities of the cationic ABTS radical are reported in Table 1.

The combined analysis indicates that the molecule remains intact without a breakage of bonds and the spin density is delocalized over the whole molecule. The PCM/DFT calculation shows that the trans ABTS conformation is the more stable radical form and that the Mulliken atomic spin densities (see Fig. 3) suggest that the molecule might approach the T1 site with a tilted structure [47]. Crystallographic data reported for the adduct of the bacterial laccase CotA and ABTS suggest a similar arrangement [53].

Vio

The CW-EPR spectra of Violuric Acid (VIO) radical, an N–OH type synthetic mediator, recorded at 9.4 and 244 GHz are shown in Fig. 4. The best fit of data at both frequencies have been obtained using the same set of magnetic parameters changing only the measuring frequency. The combined use of multifrequency EPR, pulse ENDOR, and PCM/DFT approach allows the assignment

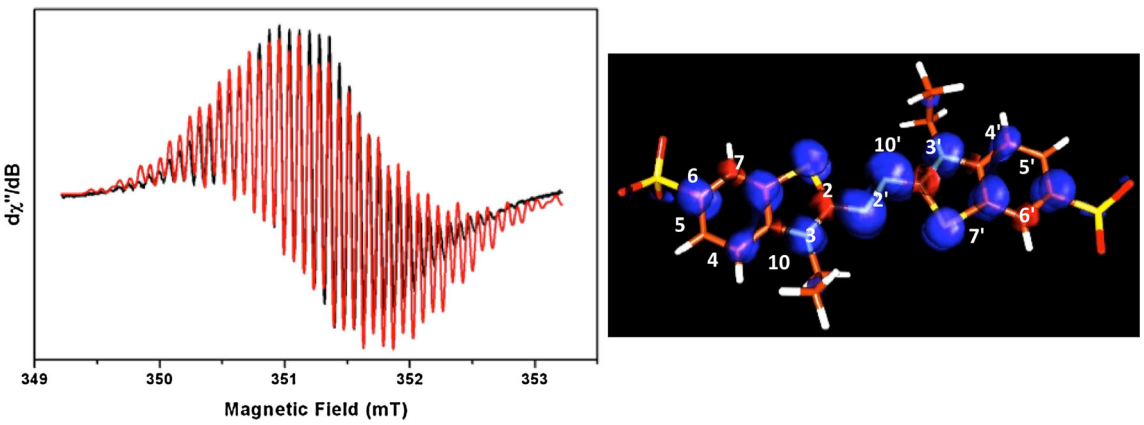

Fig. 3 *Left*. 298 K CW-EPR spectrum (X-band) of an ABTS solution formed upon oxidation by *T. versicolor* laccase (*black trace*) overlapped with its best simulation (*red trace*). The experimental parameters are as follows: 0.1 G modulation amplitude, 0.2 mW microwave power, and $\nu = 9.86$ GHz. The spectral parameters used for the simulation are given in Table 1. *Right*. B3LYP spin densities plot for the cation ABTS radical. The spin densities have been determined using a contour value of 0.003 with the program Molden [52]. *Blue* positive spin densities; *red* negative spin densities. Adapted from Brogioni et al. [47]

Table 1 Experimental and B3LYP (in water solution) *g*- and hf-tensor values for ABTS cation radical

	g_i[a]	A_i (N2) mT [c,d]	A_i (N2′) mT[c,d]	A_i (N33′) mT[c,d]	A_i (H44′) mT[c,d]	A_i (H55′) mT[c,d]	A_i (H77′) mT[c,d]	A_i (H10-10′)[b] mT[c,d]	A_i (H10-10′)[b] mT[c,d]
ABTS radical									
Experimental									
Iso[e]	2.0043	0.399	0.399	0.315	0.078	0.024	0.024	0.220	0.150
x	2.0057	1.180	1.180	0.800					
y	2.0043	0.026	0.026	0.080					
z	2.0028	0.013	0.013	0.072					
Cation radical									
B3LYP/EPRII									
Iso	2.0043	0.286	0.285	0.274	−0.085	0.008	0.048	0.237	0.121
x	2.0068	1.083	1.079	0.779	−0.026	0.036	0.093	0.321	0.226
y	2.0039	−0.106	−0.106	0.025	−0.113	0.002	0.033	0.208	0.100
z	2.0022	−0.119	−0.119	0.172	−0.117	−0.014	0.018	0.182	0.038
B3LYP/TZVP									
Iso	2.0045	0.260	0.258	0.247	−0.079	0.008	0.046	0.221	0.110
x	2.0074	1.088	1.084	−0.761	−0.022	0.035	0.091	0.305	0.215
y	2.0039	−0.148	−0.148	−0.006	−0.107	0.003	0.031	0.191	0.090
z	2.0021	−0.161	−0.162	−0.014	−0.110	−0.014	0.015	0.167	0.027

For atom numbering see Fig. 3

[a] The *g*-tensor principal values ($g_{x,\ y,\ z}$) are given with a maximum error of ±0.0001

[b] The labels "Ha" and "Hb" have been used because the hf-tensor principal values of the two protons of C10 (and also of C10′) are different

[c] Estimated error of ±0.05 mT for the hf-tensor principal components

[d] The *g*- and hf-tensor values fit the X-band and HF EPR spectra equally well (Figs. 3, 5)

[e] Isotropic values are referred to room temperature spectra

of the EPR signal to a stable neutral radical species. Having a rather asymmetric charge distribution compared to that of a cationic radical which has a more symmetric spin density distribution (see the B3LYP computed geometries and spin densities in Fig. 4c). The B3LYP/EPRII and B3LYP/TZVP *g*- and hf-tensor values for neutral and cation VIO radicals are reported in Table 2 in comparison to the experimental values. As for ABTS, the PCM has been used to simulate the bulk solvent effects. For a complete set of data (using different combinations of functionals and basis sets) and details on the B3LYP calculations see Ref. [47].

The comparison between the experimental and computational data reveals that a good agreement is found only in the case of the neutral radical. In particular, the B3LYP hyperfine-tensor values of N7 for the neutral species reproduce well the observed values that are typical of strongly coupled nitrogen. In contrast, the same values computed for the cationic structure differ more than 1 mT in comparison with the experimental ones. Similarly, from Table 2, it is evident that there is a good fit between the computed *g*-tensor values for the neutral radical and the observed ones, while the corresponding values for the cation radical are significantly larger than the experimental values. Moreover, the computed hfcc values for H7 predicted a strongly coupled hydrogen nucleus for the cation radical structure which has no correspondence in the ENDOR spectra that instead provided evidence of two coupled hydrogens with smaller hfcs [47]. In addition, the *g*- and hfc-values computed in the presence of explicit water molecules surrounding the neutral VIO radical were in poorer agreement with the experimental ones. Thus, we could conclude that the combined computational and experimental analysis of the VIO radical species strongly supports the assignment of the EPR and ENDOR spectra to a neutral VIO radical not strongly hydrogen bonded at N7.

4-methylamino benzoic acid

The radical intermediate structure involved in the *Trametes versicolor* laccase oxidation process using the 4-methylamino benzoic acid as a precursor molecule, within the synthesis of novel compounds, was determined by UV–Vis and EPR spectroscopy, combined with PCM/DFT calculations [48]. Indeed, the B3LYP/EPRII isotropic hyperfine coupling constants (hfcc) and *g*-tensor values support the assignment of the EPR signal to a dimeric cation radical species (Table 3; Fig. 5). In particular, the computed hfcc

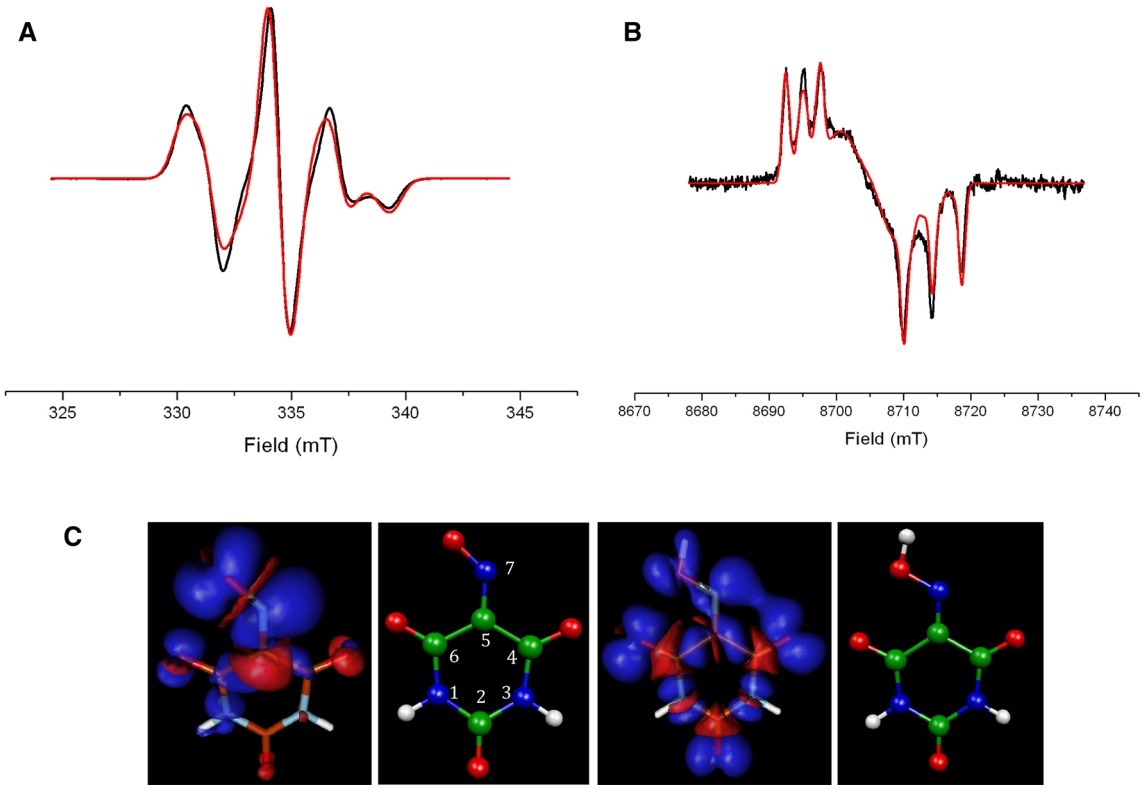

Fig. 4 CW-EPR spectra of VIO radical formed via enzymatic oxidation (*black line*) paired with its best simulation (*red line*): **a** high resolution narrow scan of the X-band EPR (modulation amplitude = 1G, microwave power = 2 mW, ν = 9.39 GHz, 100 K); **b** 243.81 GHz EPR spectrum (modulation amplitude = 10 G, microwave power = 25 mW, 8 K). **c** B3LYP molecular structures and spin densities plots for neutral (*left*) and cation (*right*) VIO radicals. The spin densities have been determined using a contour value of 0.003 with the program Molden [52]. *Blue* positive spin densities; *red* negative spin densities. Adapted from Brogioni et al. [47]

values for N7 and N7′ nucleus of the cationic structure are in good agreement with experimental values. The involvement of the dimeric radical species (both neutral and cation) has been also confirmed by the computation at the time-dependent DFT (TD-DFT) level of the absorption maxima of the two radical species. The B3LYP/6-31 + G^* vertical transition energies are 1.82 eV (cation radical) and 2.13 eV (neutral radical), in agreement with the experimental values associated to the two absorption maxima of the UV–Vis spectrum. The computed oscillator strengths are 0.39 and 0.21, respectively. For more details on the DFT and TD-DFT calculations see Martorana et al. [48].

2,6-dimethoxyphenols

Most of the mediator molecules investigated so far have been shown to be false mediators, since they are completely oxidized, removed from the cycle [54] and employed in a high molar ratio mediator/substrate [45]. Natural mediators might be more efficient, cheaper, and environmentally friendly. An ideal redox mediator has to be a good substrate, to have a stable oxidized form and its redox conversion has to be cyclic. Furthermore, for industrial application, a mediator should also be environmentally friendly and available at low cost [41, 45, 46, 55]. A great deal of interest was recently focused on the natural phenolic mediators and among lignin-derived phenols, dimethoxyphenol compounds are the fastest and most efficient [56, 57]. However, little information regarding radical structures formed during the catalytic reaction is present in literature. Electron-donating substituents on the benzene ring of phenol mediator increase laccase activity and the stability of phenoxyl radicals is improved by the steric hindrance of the hydroxyl group on the phenol [58, 59].

In this regard, a multifrequency EPR study on 2,6-dimethoxyphenol mediators, such as acetosyringone, syringaldehyde, syringaldazine, methyl syringate, and 2,6-dimethoxyphenol, in the presence of *Coriolopsis gallica* laccase has been carried out thanks to their stable radical intermediates and their well-structured and intense EPR signals. A relationship between the molecular structure of the mediator compounds and the radical characterization has been defined [33, 59]. The study began with a Structure−Activity Relationship (SAR) analysis in order to classify different phenolic mediators. Five quantum-

Table 2 Experimental and B3LYP (in water solution) *g*- and hf-tensor values for neutral and cation VIO radicals

	g_i[a]	A_i (N7) mT[b,c]	A_i (N3) mT[b,c]	A_i (N1) mT[b,c]	A_i (H1) mT[b,c]	A_i (H3) mT[b,c]	A_i (H7) mT[b,c]
VIO radical							
Experimental							
x	2.0066	2.532	0.143	ND[d]	0.050	0.128	ND[d]
y	2.0039	2.343	0.214	ND[d]	0.057	0.164	ND[d]
z	2.0020	4.589	0.268	ND[d]	0.086	0.257	ND[d]
Neutral radical							
B3LYP/EPRII							
x	2.0065	2.614	0.286	−0.020	−0.028	0.134	0.855
y	2.0034	2.430	0.297	−0.009	−0.029	0.171	0.722
z	2.0020	4.402	0.376	−0.003	0.037	0.266	1.703
B3LYP/TZVP							
x	2.0067	2.568	0.283	−0.021	−0.028	0.134	0.814
y	2.0033	2.382	0.293	−0.009	−0.029	0.171	0.679
z	2.0019	4.469	0.375	−0.003	0.037	0.266	1.678
Cation radical							
uB3LYP/EPRII							
x	2.0103	1.095	0.055	−0.154	−0.003	0.088	
y	2.0091	1.042	0.102	−0.133	−0.109	−0.133	
z	2.0037	1.785	0.427	−0.031	0.044	0.259	
uB3LYP/TZVP							
x	2.0108	1.120	0.051	−0.156	−0.003	0.074	
y	2.0094	1.060	0.100	−0.134	−0.106	−0.145	
z	2.0038	1.872	0.439	−0.031	0.044	0.246	

For atom numbering see Fig. 4

[a] The *g*-tensor principal values ($g_{x,\ y,\ z}$) are given with a maximum error of ±0.0001

[b] Estimated error of ±0.05 mT for the hf-tensor principal components

[c] Euler angles calculated with best simulations are as follows: $\theta_1 = 98.5°$, $\theta_2 = -147.8°$, $\theta_3 = -97.8°$. The *g*- and hf-tensor values fit X-, Q-band, and HF EPR spectra equally well (Figs. 2, 4)

[d] ND, not determined. N1 has hf-tensor value too small to be measured. H7 it is not present in the experimental spectra

Table 3 Experimental and B3LYP/EPRII g-tensor and hfccs values for the cation and neutral radical species

	g_{iso}[a]	AN_7[b]	$AN_{7'}$[b]	$AH_{7'}$[b]	AH_{CH3}[b]	AH_{arom}[b]
Experimental	2.0035	0.83	0.48	0.66	0.88	0.20
B3LYP/EPRII						
Cation	2.0035	0.71	0.46	−0.56	0.79[c]	−0.26[d]
Neutral	2.0037	0.34	0.81	–	0.49[c]	−0.25[d]

For atom numbering see Fig. 5

[a] Estimated error ±0.001

[b] Coupling constants are given in mT; estimated error ±0.03 mT

[c] hfcc average value for methyl protons are reported

[d] hfcc average value for aromatic protons are reported. hfcc for H_3, $H_{3'}$, H_5, $H_{5'}$ are as follows: −0.27, −0.25, −0.26, −0.26 (for the cation species) and −0.19, −0.29, −0.17, −0.34 (for the neutral species)

chemical calculated molecular descriptors (redox potential, ionization energy, enthalpy of formation of the radical, O–H bond dissociation energy) were used for the Decision tree (DT) classification models. The DT model showed that 2,6-dimethoxyphenol derivatives with a slightly electron-withdrawing substituent at the 4-position of the benzene

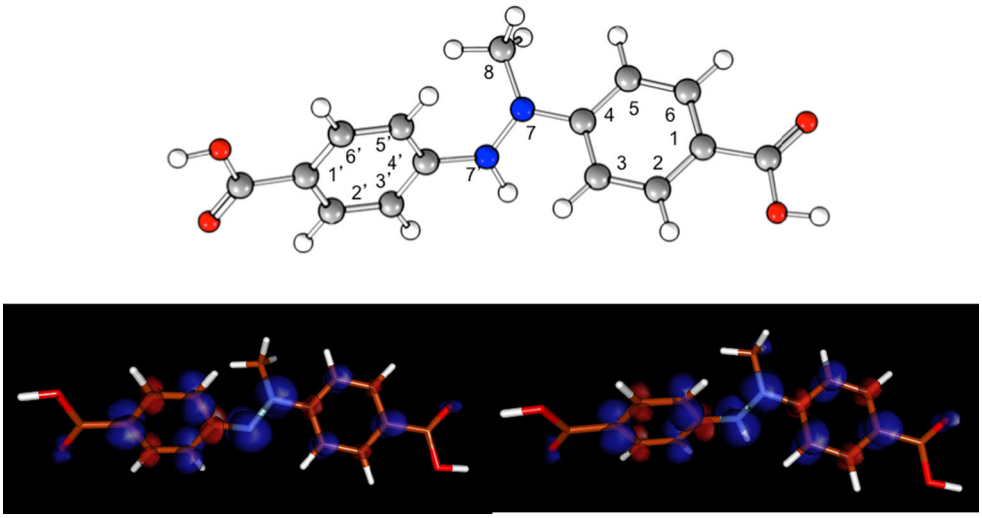

Fig. 5 B3LYP/EPRII computed molecular structure of the cationic radical dimer (*top*) and of the spin density distributions of the neutral radical dimer (*bottom*, *left*) and cationic radical dimer (*bottom*, *right*) visualized using a contour value of 0.003 with the program package MOLDEN [52]

ring were good mediators and the prediction ability was tested and confirmed with experimental data [60].

The EPR characterization of the above mentioned 2,6-dimethoxyphenol radical intermediates formed during the catalytic reaction of the *Coriolopsis gallica* was carried out and a correlation between the substituents on the aromatic ring and the signal intensity of the radical generated was obtained, pointing out the main aspects of radical stability essential to increase the mediator efficiency [33, 59]. The EPR approach was at first applied to the acetosyringone, a natural mediator, which forms a considerably stable radical and that represents a good example to build new mediator molecules. In Fig. 6, the X-band EPR spectrum (black line) paired to its simulation (red line) of the acetosyringone

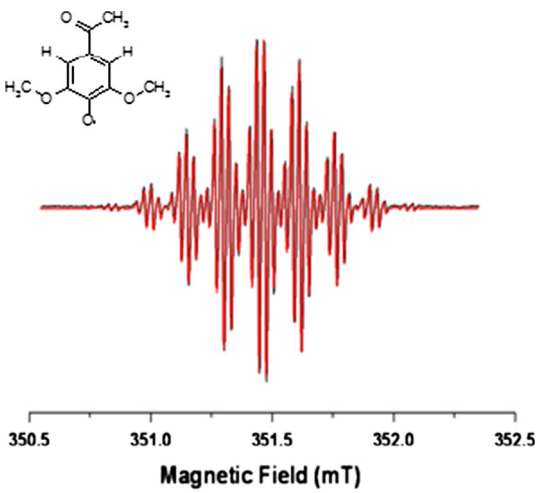

Fig. 6 CW X-band EPR spectrum of acetosyringone (*black line*) paired with its best simulation (*red line*). Experimental conditions: $\nu = 9.87$ GHz, 0.63 mW microwave power, 0.01 mT modulation amplitude, 298 K. On the left side the acetosyringone structure is reported. Adapted from Martorana et al. [59]

radical formed at room temperature after the action of the *Coriolopsis gallica* laccase is reported. The W-band spectrum recorded on the acetosyringone radical allowed investigators to resolve the g anisotropy and to measure the principal g_x, g_y, g_z values as 2.0066, 2.0053, 2.0020, respectively, and the use of the S-band frequency helped in elucidating the coupling constant assignments [59].

The spectrum reported in Fig. 6 has a $g_{iso} = 2.0045$. It was simulated considering two main hyperfine couplings: $A = 0.17$ mT belonging to two aromatic hydrogens and $A = 0.14$ mT from six equivalent hydrogens of methoxy groups. The final superhyperfine coupling with $A = 0.0029$ mT is due to three equivalent hydrogens on the acetyl group [59].

In order to study the radical stability, the acetosyringone radical was investigated versus time by EPR. The radical intermediate shows the highest intensity at $t = 0$, follows an exponential decay to a plateau after 8 min, lasting for 3 h [59, 60]. The strong signal intensity and the great stability make acetosyringone a good candidate for industrial application. One of the disadvantages related to the use of phenolic compounds in the catalytic mechanism of laccase is that the by-products formation may induce polymerization processes [61]. Therefore, the catalytic reaction was also studied by NALDI-TOF MS in order to investigate possible by-reactions. The interesting result is that after purification of the reaction solution more than 93 % of the final product is the acetosyringone itself, thus confirming the great stability of the radical, that the by-products are produced in a very low amount and that the oxidation reaction is cyclic [59]. Extending the EPR approach used for the characterization of acetosyringone, the same analysis was performed on syringaldehyde, syringaldazine, methyl syringate, and 2,6-dimethoxyphenol. Sterically hindered phenols with bulky

alkyl substituents in *ortho* to hydroxyl influence some properties of phenols [62]: the substituents avoid reactions involving the hydrogen of OH [63] and the radicals without α-H in *ortho* are extremely stable [23]. The ether oxygen may be involved in the delocalization and stabilizes the radical [64]. In Fig. 7, the X-band EPR spectra of syringaldehyde (Fig. 7a), syringaldazine (Fig. 7b), and methyl syringate (Fig. 7c) paired to their simulations have been reported [33].

The simulations were run considering two sets of protons equal for all mediators: two equivalent aromatic hydrogens with $A = 0.17$ mT and six equivalent hydrogen atoms with $A = 0.14$ mT due to the methoxy group. The different coupling constant depends on the substituent in

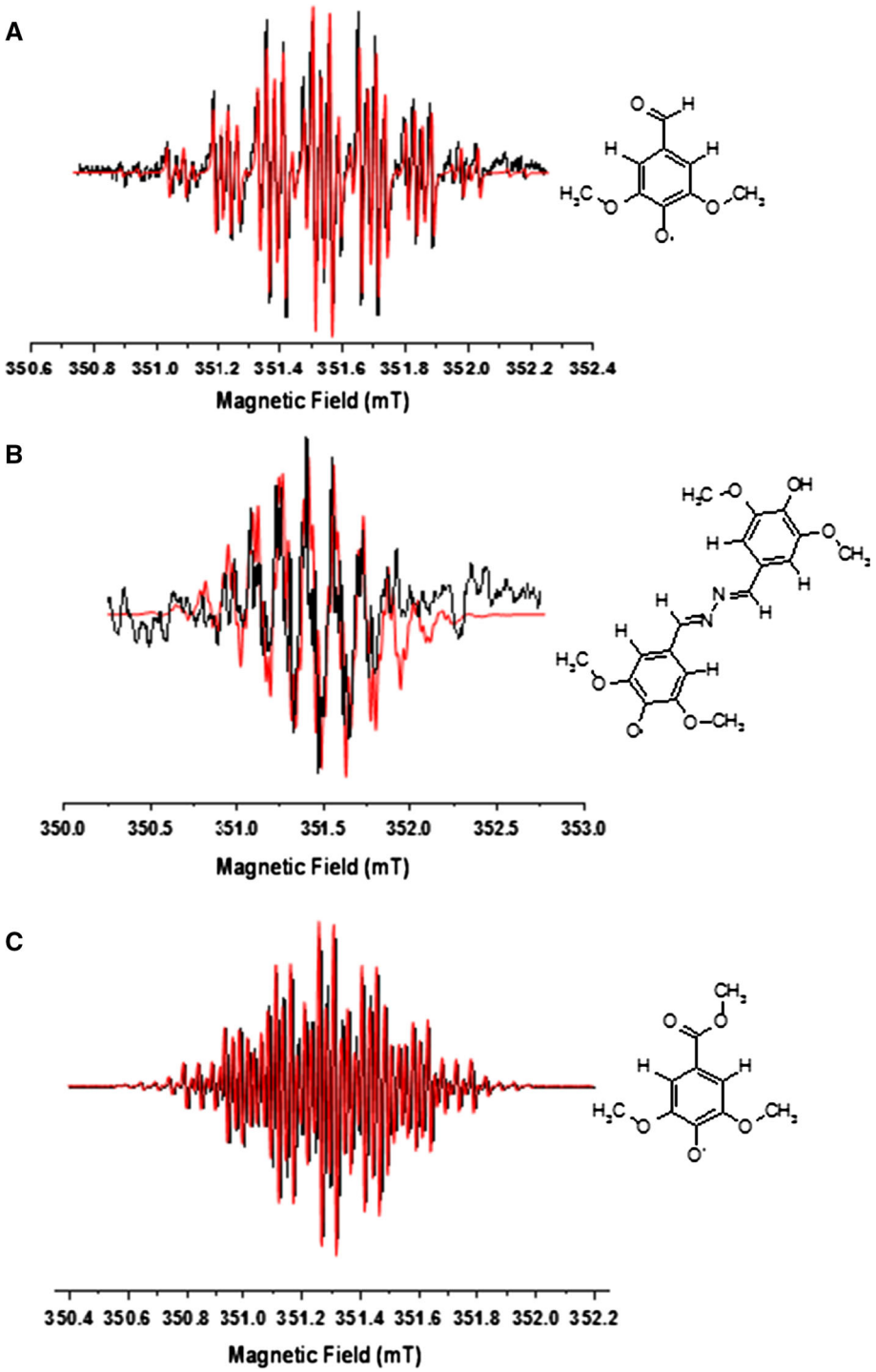

Fig. 7 CW X-band EPR spectra of the radical intermediates (*black line*) formed via enzymatic oxidation, paired with their simulations (*red line*) of: **a** syringaldehyde, **b** syringaldazine, **c** methyl syringate. Experimental conditions: 9.87 GHz, 0.63 mW microwave power, 0.01 mT modulation amplitude, 298 K. On the right side the syringaldehyde, syringaldazine, methyl syringate structures are reported. Adapted from Martorana et al. [33]

Table 4 Magnetic parameters for dimethoxyphenol mediator radicals

Mediator	g_{iso}^{a}	AH_{aromat} mT[b]	AH_{OCH3} mT[b]	$AH_{para\text{-}substituent}$ mT[b]
Acetosyringone	2.0045	0.17	0.14	0.029 (3H)
Syringaldehyde	2.0041	0.17	0.14	0.05 (1H)
Syringaldazine	2.0047	0.17	0.14	0.023 (2H) 0.028 (2 N)
Methyl syringate	2.0048	0.17	0.14	0.05 (3H)

[a] Isotropic g values (estimated error of ±0.0001) are referred to room temperature

[b] hf-tensor values are given in mT (estimated error of ±0.003 mT)

para position. In particular, in syringaldheyde, the superhyperfine coupling is $A = 0.05$ mT and comes from the interaction with the hydrogen of the formyl group; for syringaldazine, the superhyperfine structure is due to two benzylic hydrogens with $A = 0.23$ mT and two nitrogen atoms in the hydrazine group with $A = 0.028$ mT; methyl syringate, instead, has a OCH_3 substituent, therefore the spectrum was simulated with a superhyperfine coupling constant $A = 0.05$ mT due to the three equivalent H of the ester group [33].

In Table 4, the magnetic parameters obtained from the simulation of the dimethoxyphenol mediator radicals are reported.

Since the *para* position in the phenoxyl radicals represents the main site for unpaired electron delocalization, it was believed that the absence of the *para* substituent, as it occurs in the 2,6-dimethoxyphenol, would not have stabilized the radical, determining the formation of dimers and trimers. This was confirmed when recording the EPR spectrum in the presence of 2,6-dimethoxyphenol and no radical signal was detected. Such a result was also confirmed by the NALDI-TOF mass spectrum which showed a single peak with a *m/z* 305 consistent with a quinoid dimeric final product [33].

Conclusions

Chemical industry and economic development need enzymatic oxidation reactions. Still the market presents a lack of biocatalysts with the required selectivity, availability, and compatibility with the rigorous conditions applied in the chemical industry (high substrate concentrations, use of co-solvents, and high concentration of oxidants). Laccases exhibit high substrate conversion under laboratory conditions and improvement of their oxidation activity and stability take great advantage from structural–functional information. Indeed, as shown above, biocatalysts and the catalytic intermediates can be adequately characterized by a spectroscopic and computational combined approach. The in deep knowledge of structural and catalytic aspects will help in designing novel biocatalysts with improved activity.

Acknowledgments This work was supported by the PRIN 2009-STNWX3 project of the Italian Ministry of Education, Universities and Research (MIUR) and by the Eco-Innovation European Project BISCOL (ECO/09/256112). Careful reading and revising of the manuscript by Les Brooks, Chemistry Professor Emeritus, Sonoma State University, is gratefully acknowledged.

References

1. Yoshida H (1883) Chemistry of lacquer (urushi). Part I. J Chem Soc 43:472–486
2. Mayer AM, Staples RC (2002) Laccase: new Functions for an old enzyme. Phytochemistry 60:551–565
3. Shumacovich G, Streltsov A, Gorshina E, Rusinova T, Kurova V, Vasil'eva I, Otrokhov G, Morozova O, Yaropolov A (2009) Laccase-catalyzed oxidative polymerization of aniline dimer (N-phenyl-1,4-phenylendiamine) in aqueous micellar solution of sodium dodecylbenzenesulfonate. J Mol Cat B Enzym 69:83–88
4. Yaropolov AI, Skorobogat'ko OV, Vartanov SS, Varfolomeev SD (1994) Laccase: properties, catalytic mechanism and applicability. Appl Biochem Biotechnol 49:257–280
5. Xu F (1996) Oxidation of phenols, anilines, and benzenethiols by fungal laccases: correlation between activity and redox potentials as well as halide inhibition. Biochemistry 35:7608–7614
6. Messerschmidt A (ed) (1997) Multi-copper oxidases. World Scientific Singapore, Singapore
7. Gianfreda L, Xu F, Bollag JM (1999) Laccases: a useful group of oxidoreductive enzymes. Bioremediat J 3:1–26
8. Marcus RA, Sutin N (1985) Electron transfer in chemistry and biology. Biochim Biophys Acta 811:265–322
9. Xu F, Kulys JJ, Duke K, Li K, Krikstopaitis K, Deusse HJW, Abbate E, Galinyte V, Schneider P (2000) Redox chemistry in laccase-catalyzed oxidation of N-Hydroxy compounds. Appl Environ Microbiol 66:2052–2056
10. Xu F, Shin W, Brown SH, Wahleithner JA, Sundaram UM, Solomon EI (1996) A study of a series of recombinant fungal laccases and bilirubin oxidase that exhibit significant differences in redox potential, substrate specificity and stability. Biochim Biophys Acta 1292:303–311
11. Mikolasch A, Schauer F (2009) Fungal laccases as tools for the synthesis of new hybrid molecules and biomaterials. Appl Microbiol Biotechnol 82:605–624
12. Baldrian P (2006) Fungal laccases—occurrence and properties. FEMS Microbial rev 30:215–224
13. Piscitelli A, Del Vecchio C, Faraco V, Giardina P, Macellaro G, Miele A, Pezzella C, Sannia G (2011) Fungal laccases: versatile tools for lignocellulose transformation. C R Biol 334:789–794

14. Bourbonnais R, Paice MG (1990) Oxidation of non-phenolic substrates. An expanded role for laccase in lignin biodegradation. FEBS 267:99–102
15. Polak J, Jarosz-Wilkolazka A (2012) Fungal Laccases as green catalysts for dye synthesis. Process Biochem 47:1295–1307
16. Forte S, Polak J, Valensin D, Taddei M, Basosi R, Vanhulle S, Jarosz-Wilkolazka A, Pogni R (2010) Synthesis and structural characterization of a novel phenoxazinone dye by use of a fungal laccase. J Mol Catal B Enzym 63:116–120
17. Bruyneel F, Basosi R, Bols CM, Enaud E, Hercher C, Jager IJ, Marchand-Brynaert J, Pogni R, Polak J, Jarosz A, Wilkolaska A, Vanhulle S, Phenoxazine dyes. US Patent 61/078670 (2008) and 12/498,666 (2009) and PCT PCT/EP2009/058640 (2009)
18. Monti D, Ottolina G, Carrea G, Riva S (2011) Redox Chemistry catalyzed by isolated enzymes. Chem Rev 111:4111–4140
19. Wong DMS (2009) Structure and action mechanism of ligninolytic enzymes. Appl Biochem Biotechnol 157:174–209
20. Kosman DJJ (2010) Multicopper oxidases: a workshop on copper coordination chemistry, electron transfer, and metallophysiology. J Biol Inorg Chem 15:15–28
21. Reinhammar B (1984) In: Lontie R (ed) Copper proteins and copper enzymes. CRC Press, Boca Raton, p 1
22. Solomon EI, Sundaram UM, Machonkin TE (1996) Multicopper oxidases and oxygenases. Chem Rev 96:2563–2606
23. Solomon EI, Baldwin MJ, Lowery MD (1992) Electronic structures of active sites in copper proteins: contributions to reactivity. Chem Rev 92:521–542
24. Piontek K, Antorini M, Choinowski T (2002) Crystal structure of a laccase from the fungus *Trametes versicolor* at 1.90-Å resolution containing a full complement of coppers. J Biol Chem 277:37663–37669
25. Cambria MT, Gullotto D, Garavaglia S, Cambria A (2012) In silico study of structural determinants modulating the redox potential of Rigidoporus lignosus and other fungal laccases. J Biomol Struct Dyn 30:89–101
26. Yoon J, Liboiron BD, Sarangi R, Hodgson KO, Hedman B, Solomon EI (2007) The two oxidized forms of the trinuclear Cu cluster in the multicopper oxidases and mechanism for the decay of the native intermediate. Proc Natl Acad Sci USA 104:13609–13614
27. Ryde U, Hsiao Y-W, Rulíšek L, Solomon EI (2007) Identification of the peroxy adduct in multicopper oxidases by a combination of computational chemistry and extended x-ray absorption fine-structure measurements. J Am Chem Soc 129:726–727
28. Macellaro G, Baratto MC, Piscitelli A, Pezzella C, Fabrizi de Biani F, Palmese A, Piumi F, Record E, Basosi R, Sannia G (2014) Effective mutations in a high redox potential laccase from Pleurotus ostreatus. Appl Microbiol Biotechnol 98:4949–4961
29. Vänngård T (1972) In: Bolton JR, Swartz HM, Borg DC (eds) Biological applications of electron spin resonance. Wiley, New York, p 411
30. Hyde JS, Froncisz W (1982) Ann Rev Biophys Bioeng 11:391
31. Basosi R, Antholine WE, Hyde JS (2004) Multifrequency ESR of copper: biophysical applications. In: Berliner LJ, Reuben J (eds) Biological magnetic resonance. Plenum Press, New York, pp 103–150
32. Pogni R, Brogioni B, Baratto MC, Sinicropi A, Giardina P, Pezzella C, Sannia G, Basosi R (2007) Evidence for a radical mechanism in biocatalytic degradation of synthetic dyes by fungal laccases mediated by violuric acid. Biocatal Biotransform 25:269–275
33. Martorana A, Vazquez-Duhalt R, Auila SA, Basosi R, Baratto MC (2014) Spectroscopic characterization of 2,6-dimethoxyphenol radical intermediates in the *Coriolopsis gallica* laccase-mediator system. J Mol Catal B Enzym 107:100–105
34. Froncisz W, Hyde JS (1980) Broadening by strains of lines in the g-parallel region of Cu2+ EPR spectra. J Chem Phys 73:3123–3131
35. Basosi R, Della Lunga G, Pogni R (2004) Copper biomolecules in solution. In: Eaton SS, Eaton GR, Berliner LJ (eds) Biomedical EPR-part A: free radicals, metals, medicine and physiology. Kluwer Academic/Plenum Publishers, New York, pp 385–416
36. Antholine WE (2004) Low frequency EPR of Cu^{2+}. In: Eaton SS, Eaton GR, Berliner LJ (eds) Biomedical EPR-part A: free radicals, metals, medicine and physiology. Kluwer Academic/Plenum Publishers, New York, pp 417–454
37. De la Mora E, Lovett JE, Blanford CF, Garman EF, Valderrama B, Rudino-Pinera E (2012) Structural changes caused by radiation-induced reduction and radiolysis: the effect of X-ray absorbed dose in a fungal multicopper oxidase. Acta Cryst D68:564–577
38. Fernandes AT, Damas JM, Todorovic S, Huber R, Baratto MC, Pogni R, Soares CM, Martins LO (2010) The multicopper oxidase from the archaeon *Pyrobaculum aerophilum* shows nitrous oxide reductase activity. FEBS J 277:3176–3189
39. Baiocco P, Barreca AM, Fabbrini M, Galli C, Gentili P (2003) Promoting laccase activity towards non-phenolic substrates: a mechanistic investigation with some laccase-mediator systems. Org Biomol Chem 1:191–197
40. Fabbrini M, Galli C, Gentili P (2002) Radical or electron-transfer mechanism of oxidation with some laccase/mediator systems. J Mol Cat B Enzym 18:169–171
41. Camarero S, Canas AI, Nousiainen P, Record E, Lomascolo A, Martinez MJ, Martinez AT (2008) *p*-Hydroxycinnamic acids as natural mediators for laccase oxidation of recalcitrant compounds. Environ Sci Technol 42:6703–6709
42. Torres Duarte C, Roman R, Tinoco R, Vazquez-Duhalt R (2009) Halogenated pesticide transformation by a laccase-mediator system. Chemosphere 77:687–692
43. Majcherczyk A, Johannes C, Hüttermann A (1998) Oxidation of polycyclic aromatic hydrocarbons (PAH) by laccase of Trametes versicolor. Enzyme Microbial Technol 22:335–341
44. Johannes C, Majcherczyk A (2000) Natural mediators in the oxidation of polycyclic aromatic hydrocarbons by laccase mediator systems. Appl Environ Microbiol 66:524–528
45. Camarero S, Ibarra D, Martinez MJ, Martinez AT (2005) Lignin-derived compounds as efficient laccase mediators for decolorization of different types of recalcitrant dyes. Appl Environ Microbiol 71:1775–1784
46. Morozova OV, Shumakovich GP, Shleev SV, Yaropolov YI (2007) Laccase-mediator systems and their applications: a review. Appl Biochem Microbiol 43:523–535
47. Brogioni B, Biglino D, Sinicropi A, Reijerse EJ, Giardina P, Sannia G, Lubitz W, Basosi R, Pogni R (2008) Characterization of radical intermediates in laccase-mediator systems. A multifrequency EPR, ENDOR and DFT/PCM investigation. Phys Chem Chem Phys 10:7284–7292
48. Martorana A, Bernini C, Valensin D, Sinicropi A, Pogni R, Basosi R (2011) Baratto MC (2011) Insights into the homocoupling reaction of 4-methylamino benzoic acid mediated by Trametes versicolor laccase. Mol Biosyst 7:2967–2969
49. Lopez J, Yamauchi J, Okada K, Deguchi Y (1984) ENDOR study of benzothiazolone azine cation radicals by means of a TM_{110} Mode Cavity. Bull Chem Soc Jpn 57:673–677
50. Scott SL, Chen WJ, Bakac A, Espenson JH (1993) Spectroscopic parameters electrode potentials, acid ionization constants, and electron exchange rates of the 2,2′-azinobis(3-ethylbenzothiazolone-6-sulfonate) radicals and ions. J Phys Chem 97:6710–6714
51. Kim HC, Mickel M, Hampp N (2003) Molecular origin of the stability of violuric acid radicals at high pH-values. Chem Phys Lett 371:410–416

52. Schaftenaar G, Noordik JH (2000) Molden: a pre- and post-processing program for molecular and electronic structures. J Comput Aided Mol Des 14:123–134
53. Enguita FJ, Marcal D, Martins LO, Grenha R, Henriques AO, Lindley PF, Carrondo MA (2004) Substrate and dioxygen binding to the endospore coat laccase from *Bacillus subtilis*. J Biol Chem 279:23472–23476
54. D'Acunzo F, Galli C, Masci B (2003) First evidence of catalytic mediation by phenolic compounds in the laccase-induced oxidation of lignin models. Eur J Biochem 270:3634–3640
55. Gutiérrez A, Rencoret J, Ibarra D, Camarero S, Del Rio JC, Martinez AT (2007) Removal of lipophilic extractives from paper pulp by laccase and lignin-derived phenols as natural mediators. Environ Sci Technol 41:4124–4129
56. Cañas AI, Camarero S (2010) Laccases and their natural mediators: biotechnological tools for sustainable eco-friendly processes. Biotechnol Adv 28:694–705
57. Khlifi-Slama R, Mechichi T, Sayadi S, Dhouib A (2012) Effect of natural mediators on the stability of Trametes trogii laccase during the decolourization of textile wastewaters. J Microbiol 50:226–234
58. Torres-Duarte C, Aguila S, Vazquez-Duhalt R (2011) Syringaldehyde a true laccase mediator. Comments on the Letter to the Editor from Jeon, J-R., Kim, E-J. and Chang, Y-S. Chemosphere 85:1761–1762
59. Pokhodenko VD, Khizhnyi VA, Bidzilya VA (1968) Stable Phenoxy-radicals. Russ Chem Rev 37:435–448
60. Martorana A, Sorace L, Boer H, Vazquez-Duhalt R, Basosi R, Baratto MC (2013) A spectroscopic characterization of a phenolic natural mediator in the laccase biocatalytic reaction. J Mol Catal B 97:203–208
61. Medina F, Aguila SA, Baratto MC, Martorana A, Basosi R, Alderete JB, Vazquez-Duhalt R (2013) Prediction model based on decision tree analysis for laccase mediators. Enzym Microbial Technol 52:68–76
62. Marjasvaara A, Torvinen M, Kinnunen H, Vainiotalo P (2006) Laccase-catalyzed polymerization of two phenolic compounds studied by matrix-assisted laser desorption/ionization time-of-flight and electrospray ionization Fourier transform ion cyclotron resonance mass spectrometry with collision-induced dissociation experiments. Biomacromolecules 7:1604–1609
63. Denisov ET, Khudyakov IV (1987) Mechanism of action and reactivities of the free radicals of inhibitors. Chem Rev 87:1313–1357
64. Rochester CH, Rossall B (1967) Steric hindrance and acidity. Part I. The effect of 2,6-di-t-butyl substitution on the acidity of phenols in methanol. J Chem Soc B Phys Org 743–748